

# Coarse integral holography approach for real 3D color video displays

J. S. Chen,<sup>1</sup> Q. Y. J. Smithwick,<sup>2</sup> and D. P. Chu<sup>1,\*</sup>

<sup>1</sup>Photonics and Sensors Group, Department of Engineering, University of Cambridge, 9 JJ Thomson Avenue, Cambridge CB3 0FA, UK

<sup>2</sup>Disney Research, 521 Circle 7, Glendale, CA 91201-5020, USA

\*dpc31@cam.ac.uk

**Abstract:** A colour holographic display is considered the ultimate apparatus to provide the most natural 3D viewing experience. It encodes a 3D scene as holographic patterns that then are used to reproduce the optical wavefront. The main challenge at present is for the existing technologies to cope with the full information bandwidth required for the computation and display of holographic video. We have developed a dynamic coarse integral holography approach using opto-mechanical scanning, coarse integral optics and a low space-bandwidth-product high-bandwidth spatial light modulator to display dynamic holograms with a large space-bandwidth-product at video rates, combined with an efficient rendering algorithm to reduce the information content. This makes it possible to realise a full-parallax, colour holographic video display with a bandwidth of 10 billion pixels per second, and an adequate image size and viewing angle, as well as all relevant 3D cues. Our approach is scalable and the prototype can achieve even better performance with continuing advances in hardware components.

©2016 Optical Society of America

OCIS codes: (090.0090) Holography; (090.1760) Computer holography.

---

## References and links

1. B. L. Anderson and K. Nakayama, "Toward a general theory of stereopsis: Binocular matching, occluding contours, and fusion," *Psychol. Rev.* **101**(3), 414–445 (1994).
2. V. Bruce, P. R. Green, and M. A. Georgeson, *Visual Perception: Physiology, Psychology, & Ecology* (Psychology Press, 2003).
3. E. Hecht, *Optics*, 4th ed. (Addison Wesley, 2001), Chap. 10.
4. A. Macovski, "Hologram information capacity," *J. Opt. Soc. Am.* **60**(1), 21–27 (1970).
5. V. Soloviev, "Geometry of Radiation," [www.et.byu.edu/~vps/ME340/TABLES/12.0.pdf](http://www.et.byu.edu/~vps/ME340/TABLES/12.0.pdf)
6. M. Stanley, M. A. Smith, A. P. Smith, P. J. Watson, S. D. Coomber, C. D. Cameron, C. W. Slinger, and A. Wood, "3D electronic holography display system using a 100-megapixel spatial light modulator," *Proc. SPIE* **5249**, 297–308 (2004).
7. C. W. Slinger, C. D. Cameron, S. D. Coomber, R. J. Miller, D. A. Payne, A. P. Smith, M. G. Smith, M. Stanley, and P. J. Watson, "Recent developments in computer-generated holography: toward a practical electroholography system for interactive 3D visualization," *Proc. SPIE* **5290**, 27–41 (2004).
8. Z. M. A. Lum, X. Liang, Y. Pan, R. Zheng, and X. Xu, "Increasing pixel count of holograms for three-dimensional holographic display by optical scan-tiling," *Opt. Eng.* **52**(1), 015802 (2013).
9. X. Xu, X. Liang, Y. Pan, R. Zheng, and Z. A. Lum, "Spatiotemporal multiplexing and streaming of hologram data for full-color holographic video display," *Opt. Rev.* **21**(3), 220–225 (2014).
10. Y. Pan, X. Xu, X. Liang, Z. A. Lum, R. Zheng, and P. P. Mar Yi Lwin, "Large-pixel-count hologram data processing for holographic 3D display," *Proc. SPIE* **8644**, 86440F (2013).
11. T. Senoh, Y. Ichihashi, R. Oi, H. Sasaki, and K. Yamamoto, "Study of a holographic TV system based on multi-view images and depth maps," *Proc. SPIE* **8644**, 86440A (2013).
12. H. Sasaki, K. Yamamoto, Y. Ichihashi, and T. Senoh, "Image size scalable full-parallax coloured three-dimensional video by electronic holography," *Sci. Rep.* **4**, 4000 (2014).
13. Y. Takaki and N. Okada, "Hologram generation by horizontal scanning of a high-speed spatial light modulator," *Appl. Opt.* **48**(17), 3255–3260 (2009).
14. D. E. Smalley, Q. Y. J. Smithwick, and V. M. Bove, Jr., "Holographic video display based on guided-wave acousto-optic devices," *Proc. SPIE* **6488**, 64880L (2007).

15. D. E. Smalley, Q. Y. J. Smithwick, V. M. Bove, Jr., J. Barabas, and S. Jolly, "Anisotropic leaky-mode modulator for holographic video displays," *Nature* **498**(7454), 313–317 (2013).
16. Q. Smithwick, J. S. Chen, and D. P. Chu, "A coarse integral holographic display," *SID Symposium Digest of Technical Papers*, **44**(1), 310–313 (2013).
17. J. S. Chen, D. P. Chu, and Q. Smithwick, "Rapid hologram generation utilizing layer-based approach and graphic rendering for realistic three-dimensional image reconstruction by angular tiling," *J. Electron. Imag.* **23**(2), 023016 (2014).
18. Overview | DLP & MEMS (Texas Instrument)- <http://www.ti.com/lstds/ti/analog/dlp/overview.page>
19. T. Kreis, P. Aswendt, and R. Hofling, "Hologram reconstruction using a digital micromirror device," *Opt. Eng.* **40**(6), 926–933 (2001).
20. E. Buckley, "Real-time error diffusion for signal-to-noise ratio improvement in a holographic projection system," *J. Disp. Technol.* **7**(2), 70–76 (2011).
21. H. Takeya, "Formulation of coarse integral imaging and its applications," *Proc. SPIE* **6803**, 680317 (2008).
22. Using Lasers with DLP®/DMD technology, <http://www.dlinnovations.com/dli/wp-content/uploads/white-paper-using-lasers-with-dlp-dmd-technology.pdf>
23. K. Akeley, "Achieving near-perfect focus cues using multiple image planes", PhD thesis, Stanford University (2004).
24. K. Akeley, S. J. Watt, A. R. Girshick, and M. S. Banks, "A stereo display prototype with multiple focal distances," *ACM Trans. Graph.* **23**(3), 804–813 (2004).
25. H. Nishi, K. Matsushima, and S. Nakahara, "Advanced rendering techniques for producing specular smooth surfaces in polygon-based high-definition computer holography," *Proc. SPIE* **8281**(1), 828110 (2012).
26. K. Matsushima and A. Kondoh, "A wave-optical algorithm for hidden-surface removal in digitally synthetic full-parallax holograms for three-dimensional objects," *Proc. SPIE* **5290**, 90–97 (2004).
27. H. Zhang, N. Collings, J. Chen, B. Crossland, D. Chu, and J. Xie, "Full parallax three-dimensional display with occlusion effect using computer generated hologram," *Opt. Eng.* **50**(7), 074003 (2011).
28. J. Song, J. Park, H. Park, and J.-I. Park, "Real-time generation of high-definition resolution digital holograms by using multiple graphic processing units," *Opt. Eng.* **52**(1), 015803 (2013).
29. N. Takada, T. Shimobaba, H. Nakayama, A. Shiraki, N. Okada, M. Oikawa, N. Masuda, and T. Ito, "Fast high-resolution computer-generated hologram computation using multiple graphics processing unit cluster system," *Appl. Opt.* **51**(30), 7303–7307 (2012).
30. D. Abookasis and J. Rosen, "Three types of computer-generated hologram synthesized from multiple angular viewpoints of a three-dimensional scene," *Appl. Opt.* **45**(25), 6533–6538 (2006).
31. J. S. Chen and D. P. Chu, "Fast calculation of wave front amplitude propagation: a tool to analyse the 3D image on a hologram (invited paper)," *Chin. Opt. Lett.* **12**(6), 060021 (2014).
32. NTU 3D Model Database ver.1, <http://3d.csie.ntu.edu.tw/~dynamic/database/>
33. D. Y. Chen, X. P. Tian, Y. T. Shen, and M. Ouhyoung, "On visual similarity based 3D model retrieval," *Comput. Graph. Forum* **22**(3), 223–232 (2003).

## 1. Introduction

Holography uses diffraction from encoded fringe patterns to reconstruct the light wavefront of a real or synthetic scene. It can contain all the information required to reproduce every visual cue for three-dimensional (3D) images [1,2].

To create a dynamic holographic display, the holographic fringe patterns are presented on a spatial light modulator (SLM), and an updatable wavefront of a 3D image is reconstructed with suitable illumination. However, a large detailed hologram with a wide field of view requires a vast amount of information both optically and computationally, making holographic video challenging to realize.

To create a large hologram with a wide field-of-view (FOV), the spatial period of the fringes must be small ( $<1 \mu\text{m}$  fringe period for  $\sim 30^\circ$  diffraction angle) and maintained over a large area (e.g.  $127 \text{ mm} \times 100 \text{ mm}$ ). The division of the hologram's spatial extent by the finest fringe period (inversely proportional to the FOV) is a dimensionless number called the space bandwidth product (SBP):

$$SBP = \frac{4 \times w \times h}{d_w \times d_h} \quad (1)$$

where  $w$  is the width of the hologram,  $h$  is the height of the hologram,  $d_w$  is the fringe period in the horizontal (width) direction, and  $d_h$  is the fringe period in the vertical (height) direction.

The SBP is equal to the maximum number of addressable points (points that could potentially be resolved or created) in an imaged plane. The SBP also relates to the maximum

number of addressable voxels by the hologram, and hence the information content of the hologram. For an analogue hologram with a SBP of  $N^2$ , the number of addressable voxels is  $N^3/3$  [3]. We are interested in the potential voxel resolution of the reconstructed 3D volume.

The SBP is related to the etendue ( $A\Omega$ ) or optical extent of the reconstructed light controllable by the hologram. For a hologram of projected area  $A$ , emitting into a solid angle of  $\Omega$  [4] with a rectangular field of view, the optical extent is equal to:

$$A\Omega = w \times h \times \cos \Phi \times (\phi_2 - \phi_1) \times (\cos \theta_2 - \cos \theta_1). \quad (2a)$$

where  $w$  and  $h$  are hologram width and height respectively;  $\phi_2$  and  $\phi_1$  are horizontal diffraction range boundaries;  $\theta_2$  and  $\theta_1$  are vertical diffraction range boundaries;  $\Phi = (\phi_2 + \phi_1)/2$  is the central angle of the diffraction range relative to the hologram's surface normal.

For a solid angle of a rectangular field of view with a small vertical field of view<sup>nl</sup>, this can be approximated as:

$$A\Omega = w \times h \times \cos \Phi \times \Delta\phi \times \Delta\theta. \quad (2b)$$

where  $\Delta\phi$  is the horizontal (azimuthal) diffraction range bound by  $[\phi_1, \phi_2]$  and  $\Delta\theta$  is the vertical (polar) diffraction range bound by  $[\theta_1, \theta_2]$  for the solid angle  $\Omega$  described in spherical coordinates.

The hologram's horizontal and vertical diffraction ranges are governed by the diffraction equation [5]:

$$\theta = \sin^{-1} \left( \frac{m \cdot \lambda}{d} + \sin \theta_i \right). \quad (3)$$

where  $\theta$  is the diffraction angle of the diffraction order  $m$ ,  $\lambda$  is the illumination wavelength,  $d$  is the fringe period and  $\theta_i$  is the illumination angle of the reconstruction beam.

The hologram's optical extent is therefore also defined by the hologram's area and fringe period, and related to its SBP.

Unfortunately, common SLMs used to present synthetic holograms have limited SBPs, equivalent to the total number of addressable SLM pixels. Commodity SLMs, such as digital micro-mirror devices (DMDs) or liquid crystal on silicon (LCOS) devices, are typically pixelated with pixel pitches only as coarse as 5-10  $\mu\text{m}$  and are the same horizontally and vertically.

Furthermore, the pixel pitches are only typically maintained over a  $\sim 20 \text{ mm} \times 20 \text{ mm}$  device. Since at least two pixels are needed per fringe period, the coarse pixel pitch and small area results in small field of view and a low SBP. Optics can increase the FOV but only at the expense of the image size, and vice versa, due to the optical invariant; the optics do not change the optical extent nor the SBP of the system. These pixelated SLMs often have quantized modulation levels, and care must be taken to ensure they have the ability to present all the information contained in the desired hologram.

Over the years, various methods have been proposed to overcome this challenge of using SLMs with limited SBPs in holographic displays, but lately there has been remarkable progress towards the realization of such apparatus. The two main approaches are to spatially tile multiple SLMs or SLM images, or to create new modulators with larger SBPs.

The QinetiQ holographic display spatially tiled multiple images of an electrically addressed SLM (EASLM) onto an optically addressed SLM (OASLM) using a shuttered lens array acting as replication optics [6,7].

A\*STAR's system combines more than twenty commodity SLMs to increase the total SBP to deliver large 10" wide colour holographic video with a limited viewing angle [8,9]. A\*STAR concurrently uses more than twenty graphic cards to compute the holographic content [10].

The National Institute of Information and Communications Technology (NICT) created holograms on their custom developed  $8k \times 4k$  multi-level phase-only SLMs, which represent the largest SBP for a single digital SLM to date [11,12].

There are also horizontal parallax only (HPO) holographic displays. The Tokyo University of Agriculture and Technology (TUAT) display uses a DMD, a scanner, and a pulsed laser to spatially tile overlapping holographic images [13]. The Mark series holovideo systems from the Massachusetts Institute of Technology (MIT) use custom acousto-optic modulators (AOM) to create long streams of fine pitched traveling fringes that are de-scanned, tiled and de-magnified [14,15].

While HPO holograms require significantly lower computation and bandwidth to display than full parallax holograms, they exhibit inherent astigmatism limiting reconstruction depth. Also the appearance of a HPO hologram does not change with vertical motion of the viewer's viewpoint. In applications involving interaction with the hologram or multiple collaborative viewers, even a small amount of vertical parallax is necessary for the viewers to perceive a consistent realistic scene.

However, even in current full parallax holographic displays providing different information content and different fields-of-view in the horizontal and vertical directions is difficult. With common square pixel SLMs, the horizontal and vertical pixel pitches, and therefore fields-of-view, are the same. In many cases, especially with limited resources, it would be desirable to have more information and wider fields of view in the horizontal direction.

We select several important existing full parallax holographic video systems in Table 1 for comparison, in which our system is included and will be introduced with more details in later sections. In Table 1, "SLM bandwidth" is the maximum total number of pixel bits per second provided by the combination of SLMs (pixels per pattern  $\times$  pattern rate); "effective bandwidth" is the equivalent number of pixel bits per second necessary to provide the achieved display performance (bits per pixel  $\times$  pixels per pattern  $\times$  pattern rate  $\times$  number of colours).

Because the optical extent and effective bandwidth in a HPO system are not comparable with those of a full parallax holographic display system, in this paper we focus on full parallax holographic displays. However, even with the remarkable progress of these displays towards large holographic video, we are still far away from the ideal holographic display.

The dynamic Coarse Integral Holographic Display (CIHD) as proposed here uses opto-mechanical scanning and coarse integral optics to angularly tile an array of holograms created by a single low SBP but high information bandwidth (SBP  $\times$  pattern rate) modulator. The resulting combined full-parallax holograms have a larger SBP produced at video frame rates.

**Table 1. Comparison of existing holographic video displays.**

System	SLM	SBP of device pattern ( $\times 10^6$ bits)	Number of Devices	SLM Bandwidth per device ( $\times 10^9$ bits/sec)	Effective Bandwidth ( $\times 10^9$ bits/sec)	Hologram Tiling Structure	Algorithm
QinetiQ (2004) [6,7]	FLCOS	~1.0	4	~0.8	~3	Spatial	Point-based
A*STAR (2013/14) [8-10]	FLCOS	~1.3	24	~0.924	~22.4	Spatial & Temporal	Point-based
NICT (2014) [11]	LCOS	~33.2	3	~2.0	~6	Spatial	Point-based
Dynamic CIH (2015/16)	DMD	~0.8	1	~17.8	~10	Angular	Layer-based

Cell shading: dark: preferred; medium: acceptable; light: limited. FLCOS stands for ferro-electric LCOS.

The display system to be presented in section 2 is the dynamic version of our previous work [16], while the algorithm [17] used in this work will be discussed in more together with our view on information calculation details in section 6.

## 2. Coarse integral holograms

In 2013, we introduced a method of angularly tiling several low SBP holograms to form a modest size, full parallax hologram with a wide horizontal field-of-view and some vertical parallax. The information can be flexibly distributed and adjusted separately between the horizontal and vertical fields-of-view. This solution is produced by combining holograms and coarse integral optics into a Coarse Integral Holographic Display (CIHD) [16]. The low SBP holograms provide a set of full 3D images but each with a small area and a small field-of-view. Each hologram reproduces a different narrow viewpoint of the same 3D scene. The coarse integral optics angularly tiles the multiple narrow field-of-view holograms into a single large field-of-view hologram.

Previously reported results of the CIHD used a static array of holograms recorded as a binary mask. To create a dynamic hologram by tiling multiple SLMs would be expensive and may underutilize the bandwidth of each SLM.

Our proposed solution in this work is to angularly combine several low SBP holograms from a single scanned high-pattern rate SLM into a modest size wide field-of-view full parallax hologram at video frame rates. R/G/B colours are realised using time-multiplexing which can further take the advantage of the SLM's high bandwidth.

We also implement a multi-view multi-layer hologram rendering algorithm on the holographic video system to achieve the rapid hologram generation [17].

To make our system more understandable, we discuss the information content in a holographic display. We describe how information contained in a desired analogue hologram is affected and reproduced when presented on a pixelated binary SLM with limited information but high bandwidth capabilities, and combined using opt-mechanical and optical systems. We further describe how the rendering algorithm works with the hardware to remove unused or redundant information to reduce the computational load.

## 3. Information content and the holographic display

### 3.1 Information content and optical extent

To address the motivation behind our optical system clearly, we calculate the optical extent, imaged volume resolution, and information content of a desired hologram and of a common SLM.

For example, a SLM of  $1,024 \times 768$  resolution with a pixel pitch size of  $10 \mu\text{m}$  would have a  $10.24 \text{ mm} \times 7.68 \text{ mm}$  area. A hologram presented on the SLM, with at least two pixels per finest fringe period, would have a diffraction range of  $1.81^\circ \times 1.81^\circ$  about the centre of the field of view for  $633 \text{ nm}$  laser light source based on the diffraction equation Eq. (3). From the total number of SLM pixels, its SBP is equal<sup>n2</sup> to  $0.78 \times 10^6$  and from Eq. (2b), its optical extent<sup>n3</sup> is  $257.64 \text{ mm}^2 \cdot \text{deg}^2$ .

Optical demagnification may increase the field of view, but only at the expense of the hologram size; the SBP and the optical extent remain constant. In order to have a larger hologram size, say  $50 \text{ mm} \times 40 \text{ mm}$ , and wider diffraction ranges of, say  $10^\circ \times 5^\circ$ , would require an optical extent of  $\sim 10^5 \text{ mm}^2 \cdot \text{deg}^2$ , which is approximately 388 times that of a single SLM pattern. Such a large hologram would require integrating 388 of the previous holograms each with a pixel resolution of  $1,024 \times 768$  together, regardless of their pixel pitch and/or optical demagnification.

### 3.2. SLM and information capability

There are many SLM candidates able to provide the holographic fringe patterns, such as LCOS, ferro-electric LCOS (FLCOS), and DMDs. These SLMs are all pixelated with similar SBPs, as their sizes (extents) and pixel pitches are typically optimized for similar uses in the display and projection industries. Essentially, the device's SBP is related to its total number of pixels, and its potential information content related to the product of its SBP and number of bits per pixel. However these SLMs differ in the type of modulation, number of modulation levels, and bandwidth (specifically bits per second).

LCOS and FLCOS are phase modulation devices. LCOS can support multi-level phase modulation but at a low pattern rate (<100 Hz). FLCOS only supports binary phase modulation but is capable of kHz pattern rates. A DMD is a binary amplitude modulator working in a reflection mode and can operate at up to 32 kHz pattern rates [18]. Currently, a DMD can be driven faster than an FLCOS device because the DMD's driving electronics are more developed for the available commercial market.

The different levels of modulation are often used to control the amplitude of the holographic fringes and thereby the intensity of image voxels. Therefore these different SLMs may also have different information capabilities (information bits per pattern) and bandwidths (bits/sec) even with the same SBP.

However, it is also known that binary quantized holograms (two amplitude or phase modulation levels; e.g. clear and opaque, 0 and  $\pi$  radians of phase) are capable of producing greyscale 2D imagery or 3D holographic image [19], though the resulting greyscale image will be noisy due to the inexact conversion of a complex-valued (amplitude and phase) hologram to an either amplitude-only or phase-only fringe pattern presented on the SLM. A common technique to ameliorate the noise is to add random phase perturbations over several patterns, thus changing the noise distribution for each pattern, which is averaged over time [20]. Discrete binary holograms are of interest because many of the high-pattern rates SLMs operating in the kHz pattern rates, such as FLCOS and DMDs, only provide binary modulation.

Although a hologram presented on a binary SLM has the potential of addressing all the voxels defined by the hologram's extent and fringe period, this type of SLM's information capability is often much less than that of the hologram of similar spatial extent and fringe period but presented on an SLM with multi-level modulation control of each pixel; i.e. the voxels may be addressable based on the pixel pitch and extent of the SLM, but they are not all accessible at the same time due to the binary modulation and limited information capabilities of the SLM. For instance, a binary DMD SLM of  $1,024 \times 768$  XGA resolution only has information capability of  $(1,024 \times 768 \times 1)$  bits per pattern; while a greyscale LCOS XGA SLM has  $(1,024 \times 768 \times 8)$  bits per pattern.

To present greyscale holographic images using a binary device, we must consider the additional information required to modulate the voxels intensities. Although the binary hologram presented on the binary DMD may produce a greyscale holographic 3D image, it is at the expense of the number of voxels the DMD can simultaneously access. For instance, if we wish to have 256 grey levels (8-bits) in a holographic 3D image, we have to reduce the number of 3D points simultaneously accessible by the binary hologram by a factor of 8; only 1/8th of the voxels may be on at a time due to the conservation of information. It should be noted that this redistribution of information is only applicable from the number of bits to the number of image grey levels (no matter the SLM pixel is binary or with grey levels). We cannot transfer information from the number of hologram pixel grey levels into addressable voxel resolution nor the optical extent (field of view or spatial extent), since these are determined only by the fringe period and area of the hologram.

However, the DMD has a high bandwidth as its advantage. A high definition DMD can be driven at a 23 kHz pattern rate, with a bandwidth<sup>n4</sup> of  $47.99 \times 10^9$  bits/sec. Comparatively, a

HD LCOS can be driven at  $\sim 100$  Hz pattern rate, and therefore has a bandwidth<sup>n5</sup> of  $1.66 \times 10^9$  bits/sec, which is less than 4% of the HD DMD device. Therefore, we can use the high bandwidth of the low SBP / high bandwidth DMD to temporally multiplex multiple holograms each presenting a subset of the desired points in the greyscale (or colour) holographic image, while still achieving an overall holographic image update period of less than 1/20 second.

It is therefore apparent that we may encode our holographic fringe patterns as pixelated binary holograms, present them on a low SBP / high bandwidth binary SLM to produce greyscale or colour 3D holographic images.

### 3.3. Optical configuration: angular tiling

To fully take advantage of an SLM with a high bandwidth but low SBP, we require a device to temporally multiplex and distribute information as necessary over one update period.

Instead of using spatial tiling, as shown in Fig. 1(a), we use angular tiling, as shown in Fig. 1(b) using coarse integral holography [21], as shown in Fig. 1(c). To implement angular tiling, we display a hologram on the SLM, and then use a 4f optical relay with a two-axis scanning system at the Fourier plane to create a spatial array of SLM/hologram images behind a corresponding lenslet array. The lenslet array and a single common transform lens form a coarse integral optical system, which relays and angularly tiles the sub-holograms. The lenses and scanning mirror must be able to accept the optical extent of the light diffracted by the hologram and the SLM.

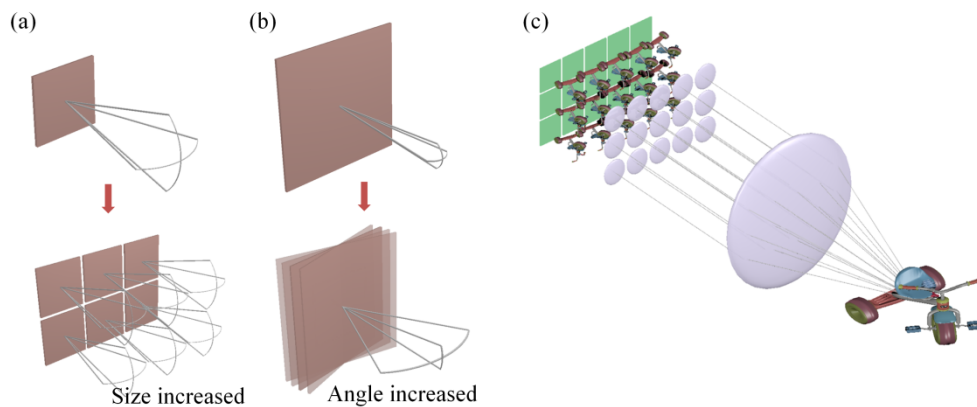


Fig. 1. An illustration of hologram tiling schemes; (a) Spatial tiling, which enlarges the effective display size by tiling many sub-holograms spatially; (b) Angular tiling, which enlarges the effective viewing angle by tiling many sub-holograms angularly; (c) Illustration of static coarse integral holography.

A rectangular array of elemental holograms supports different horizontal and vertical viewing angles, and allows more efficient use of information, since the required horizontal viewing angle is usually wider than vertical viewing. Manufacturing and alignment of a custom lens array with a large number of lens elements can be expensive and difficult. Noticing each holographic sub-hologram is paired with a corresponding lenslet; we can use the galvanometric scanner to scan a single SLM and its corresponding lenslet into a SLM/lenslet array behind the final transform lens. Furthermore, the lenslet may be a holographic lenslet that is computed and added to the holographic pattern displayed on the SLM [17].

The simplicity of the system configuration using a scanned combination of SLM with an attached holographic lens to form a sub-hologram and lenslet array warrants its use in this initial development. This particular configuration appears equivalent to imaging the

holographic image on the scanner, having the scanner angularly tile the holographic image, and then relaying and scaling the angularly tiled holographic image as a real image. The use of the attached holographic lens and design based on the CIH concepts are important to this configuration, and thus it can be considered a subset of coarse-integral holography. One disadvantage of this configuration over the general scanned CIH system with physical lenslet array is that the holographic image appears on the scan mirror preventing the ganging of multiple scan mirrors to increase the size of the scan plane without introducing seams into the holographic image. Future work will address scaling and seamlessly tiling multiple systems to form an even larger wider field of view holographic image.

### 3.4. Scanning pattern and colour scanning

To maximize the use of scanner's capabilities and make the scanning pattern efficient, bi-directional boustrophedonic scanning and view-sequential colour are used, as shown in Fig. 2. This minimizes the overlapping scanning regions and avoids horizontal and vertical flyback regions.

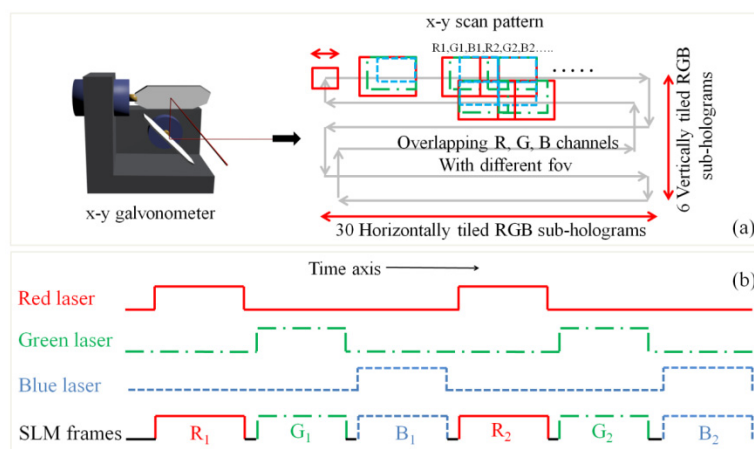


Fig. 2. (a) Illustration showing the bi-directional boustrophedon scanning with overlapping colour sub-hologram fields. The fields of view of each (RGB) channel are different. The FOV of the blue field is set to be the overall effective size—the blue constraint. In the figure, the squares' shapes and sizes are used to represent the FOVs; (b) The RGB laser pulses are applied sequentially and synchronized with SLM patterns.

Each colour holographic frame consists of a set of red, green and blue frames, and we temporally multiplex the colour components view-sequentially while scanning, as shown in Fig. 2. The laser signals for RGB components are synchronized with the SLM patterns, which are displayed in RGB order. As they are scanned, colour component sub-holograms overlap the previous component by 1/3 width of a blue frame. The rendering algorithm takes this shift (equivalent to a change in view direction between colour components) and scan direction into account. However, from Eq. (3), we see the diffraction angle is proportional to the illumination wavelength. Therefore, the blue component's holographic fringes produce holographic images with the same size but a smaller viewing angle than other colour components' fringes. The blue 3D image's field of view is about two-thirds that of the red's field of view. As we wish all the colour components to have the same visible field of view, we truncate the red and green images' fields of view to that of the blue image's field of view by blanking the corresponding portions of their sub-holograms. See Fig. 2.

## 4. Implementation, apparatus and performance

The constructed apparatus consists of a high pattern rate, low SBP (small area and coarse pixel pitch) SLM, transform optics, a 2-axis galvanometer to tile the SLM/lenslet images, and a large common transform lens to perform the angularly tiling. See Fig. 3(a) and 3(c).

Sub-holograms with attached holographic lenslets are displayed on the  $1,024 \times 768$  binary DMD (Discovery Kit, Texas Instruments) with a  $14.0 \text{ mm} \times 10.5 \text{ mm}$  area,  $13.68 \mu\text{m}$  pixel pitch and 22,727 Hz maximum pattern rate. The DMD is illuminated by red (632 nm), green (532 nm), and blue (450 nm) laser diodes (Laser Components, UK) view sequentially. The illumination's angle of incidence is  $\theta_i = 12^\circ$  with respect to the DMD's surface normal. For this illumination condition and the angle of DMD micro-mirror's on-state tilt [22], the 4th diffraction order has the greatest diffraction efficiency and its field of view is also centred<sup>n6</sup> about the DMD's surface normal,  $\Phi = 0^\circ$ . For these reasons, the 4th diffraction order is used for viewing in this system. Its diffraction range is  $2.67^\circ$ <sup>n6</sup>.

The transform optics image the holographic image on the galvanometer's mirror. To best balance filling as much of the mirror aperture with as much of the projected SLM area as possible, the SLM pattern is magnified to  $24.7 \text{ mm} \times 24.7 \text{ mm}$ , with a corresponding decrease in the viewing angle to  $\pm 0.53^\circ \times \pm 0.40^\circ$  for 450 nm light. The diagonal of this square area is slightly longer than the aperture diameter. We use a 2-axis scanner (Nutfield), with a 30 mm round mirror aperture supporting 1st axis scanning at 70 Hz for  $\pm 12^\circ$  optical scanning angle. The scanning speed is equal to  $3,360^\circ$  per second.

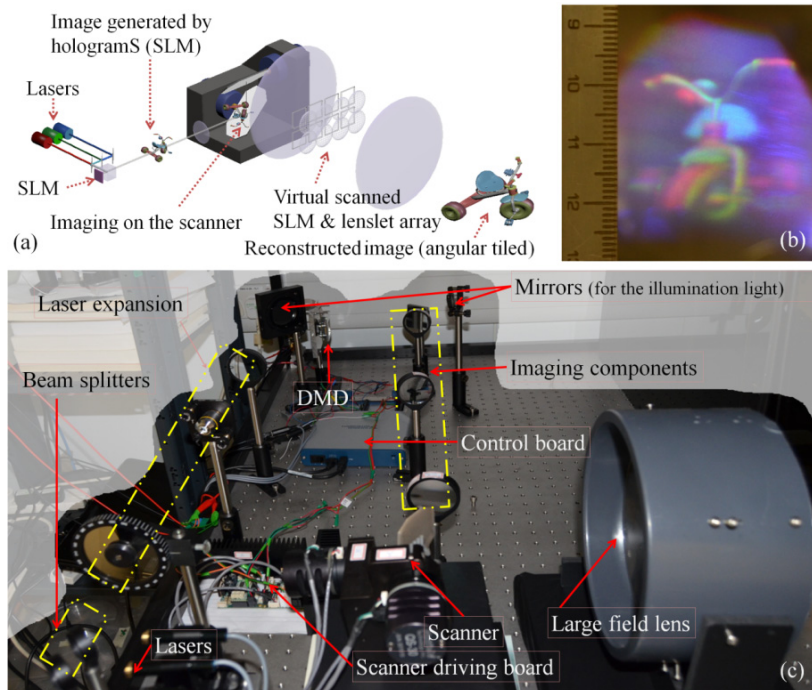


Fig. 3. Illustrations for the scanning structure and the dynamic CIH system. (a) The dynamic CIH system layout ;(b) A displayed holographic image, ruler unit in cm; (c) The physical CIH system hardware.

## 5. Hardware discussion

### 5.1 Hardware specifications

Overall, 96% of the DMD's pixels are being used to display the holographic fringes and 83% of the mirror's area is used for scanning, due to the square DMD projection on a round mirror

aperture. The  $\pm 12^\circ$  optical scanning angle can tile 30 sub-holograms per row ( $\pm 0.4^\circ$  each) horizontally. With the sub-holograms scanned into six vertical rows, we gain six vertical sub-holograms ( $\pm 0.53^\circ$  each). The array of sub-holograms and lenslets is angularly tiled with a  $2 \times$  magnification imaging lens pair. With the entire 22 kHz pattern rate of DMD SLM in use, the final angularly tiled hologram has a  $49.4 \text{ mm} \times 49.4 \text{ mm}$  aperture with a maximum central viewing angle of  $\pm 6^\circ$  horizontal  $\times \pm 1.6^\circ$  vertical, as shown in Table 2.

**Table 2. Specification of proposed holographic video system.**

Image size	$49.4 \text{ mm} \times 49.4 \text{ mm}$
Central viewing angle	$\pm 6^\circ \times \pm 1.6^\circ$
Number of tiled sub-holograms	$30 \times 6 = 180$
Frame rate	23.33 fps
Colours ( $\lambda$ )	R(632nm)/G(532nm)/B(450nm)
SLM Bandwidth ( $\times 10^9$ bits/sec)	(Max.) $17.8 \times 10^9$ bits/sec
Optical extent	$23,430 \text{ mm}^2 \text{deg}^2$
SBP	$141.6 \times 10^6$
DMD bandwidth efficiency	53.2%

### 5.2 SLM bandwidth efficiency

For each holographic frame, a set of 30 horizontal  $\times$  6 vertical sub-holograms are scanned in each of three colours. Using the entire XGA DMD as the SLM, the pixel count<sup>n7</sup> of each holographic frame is  $141.6 \times 10^6$  pixels. To provide a 23.33 Hz hologram frame rate, the horizontal scan frequency is 70 Hz and the DMD's pattern rate is equal<sup>n8</sup> to 12,600 patterns per second or approximately 10 billion pixels per second ( $9.91 \times 10^9$  pps). The DMD's maximum pattern rate is 22,727 Hz, so only<sup>n9</sup> 55.4% of the DMD's maximum bandwidth is used. However, since only 96% of the DMD's pixels are used to display holographic fringes, the actual DMD's maximum bandwidth is 53.2%

The SBP of this hologram is  $141.6 \times 10^6$  and has an optical extent of  $23,430 \text{ mm}^2 \text{deg}^2$  (at 23.33 Hz). For comparison, a hologram on a single XGA resolution DMD pattern with a  $10 \mu\text{m}$  pixel pitch (and assuming a blue-constrained system) has a SBP of  $0.78 \times 10^6$  and an optical extent of  $43.3 \text{ mm}^2 \text{deg}^2$  (at 22,727Hz). Although our single angularly tiled holographic frame may contain vastly more information than a single DMD pattern, for a dynamic holographic display we are still only able to use 53.2% of the DMD's capabilities. The DMD's reduced effective efficiency is due to the limitations of the scanner's bandwidth. For this particular scanner model's design, we fill a majority of the scanner mirror's area and use a scan angle necessary for the desired number of scan lines; the scanning speed is the main limitation. The scanner has an average rotational velocity of 3360°/sec. It takes 238  $\mu\text{s}$  for the mirror to rotate  $0.8^\circ$  of the blue frame's horizontal field of view at the scanner mirror. Using three SLM patterns (RGB) per colour hologram frame reduces the required SLM pattern period to 79  $\mu\text{s}$ . This pattern period still hasn't reached the capability of the DMD SLM of 44  $\mu\text{s}/\text{pattern}$  ( $= 22,727 \text{ Hz}$ ). Future work will examine ways to increase the scanner's bandwidth. For example, a scanner with mirrors of lighter material, such as beryllium, may increase the scanning capabilities by a factor of 1.5 to 2.

In our system, we use a SLM with a XGA resolution, and each single pattern can project a 3D image in a volume of  $49 \text{ mm} \times 49 \text{ mm} \times 49 \text{ mm}$  with viewing angle of  $0.8^\circ \times 0.66^\circ$  (based on the diffraction of blue light). The depth of the volume is arbitrary, chosen mainly to present a cubic volume and to prevent significant vignetting of deep objects within the limited field of view of the low SBP holograms. For this system, at a depth of 49 mm, the voxel resolution is still sufficient to present a contiguous high resolution 3D image.

Although the vertical field of view is small, the main intent is to provide 3D content with horizontal parallax and a definitive and consistent location in space (not provided by HPO displays). Further improvements in the scanner's bandwidth, SLM bandwidth, and/or scaling or tiling multiple SLMs and scanning systems will increase hologram's horizontal and/or vertical field of view, image size, and/or frame rate.

## 6. The rendering algorithm

Calculating holograms for 3D images requires enormous computation load, and the main goal of developing an effective and fast algorithm here is to reduce the information involved while retain all the 3D cues. It is also important to be compatible with a variety of source contents (3D models or live captures) and different display systems. Such a rendering algorithm was previously described [17], using an image-based multi-view multi-layer holographic rendering scheme. Here we look at the information content of a holographic 3D image and the simplifications that a rendering algorithm may employ to efficiently encode that information into the holographic fringes.

To understand this difficulty better, we can start by describing 3D images with a simplified model to be displayed on the previously described hardware. Imagine a spatial grid, which has a resolution of  $1,024 \times 768 \times 1,000$  voxels ( $1,024 \times 768$  resolution plane chosen due to the resolution of our DMD and a 1,000 planes to make the depth resolution similar to the horizontal resolution) over a  $49 \text{ mm} \times 49 \text{ mm} \times 49 \text{ mm}$  cubic volume. A spatial distribution of voxels is able to reconstruct a spatial 3D image, just like a volumetric display. Unfortunately, a binary SLM with  $1,024 \times 768$  pixels may only contain  $1,024 \times 768$  bits of information (it only has control of  $1,024 \times 768$  independent variables or pixels), and therefore can only simultaneously render a limited number of voxels in the volume for each pattern. Fortunately, the shortage of information per pattern on a binary device is compensated by its rapid pattern rate (i.e. large bandwidth).

Continuing our grid example, assume the horizontal and vertical fields of view are divided into 50 horizontal  $\times$  30 vertical viewpoints for each voxel, to provide smooth parallax and changes in view dependent lighting, shading and occlusion effects. Overall, the necessary bandwidth with discretized views<sup>n10</sup>, regardless of the implementation, is now  $\sim 2.35 \times 10^{14}$  bits per second (bps) simply based on the information considerations. The total amount of information to simultaneously address and render every voxel, view, and grey level in this volume for every frame is unmanageable with current technology.

Fortunately, we can make simplifications and remove redundancies and unseen content to make the rendering load more manageable. We may remove voxels from internal, occluded, and back facing volumes and surfaces since they aren't seen from a small field of view around a given rendered viewpoint. For small fields of view around that rendered viewpoint, the object will appear solid and can also provide accommodation cues while requiring at most only  $1,024 \times 768$  voxels, although with each voxel free to occupy any depth. The  $1,024 \times 768$  pixel binary SLM is capable of reproducing such a small FOV 3D image. The binary device can also achieve grey level voxel projection providing the overall bandwidth is sufficient (and each pattern is displayed fairly quickly, see section 3.2).

Furthermore the human visual system's depth resolution with accommodation is relatively low [23,24]; therefore we can degrade the 3D image's resolution in depth down to, for example, 1 cm per layer at arm's reach viewing distance (60 cm), while still maintaining a realistic contiguous perception of depth.

These simplifications, however, only work for a small field of view before they break down. View dependent holographic imagery is difficult to produce and also computationally expensive when achieved by eliminating portions of the holographic fringe patterns corresponding to undesired diffraction into certain view angles even when multiple GPUs are used [10,25–29].

We take advantage of the nature of angularly tiled CIH holograms to produce view-dependent holograms. Each voxel projected by a sub-hologram calculated by the layer-based method emits light isotropically within its view zone's small field of view. The coarse integral optics provides angularly tiled view zones independent of each other. The independence of the view zones allows each sub-hologram to be computed separately, independently of other sub-holograms for efficient and parallel computation. This allows us to render and display occlusion /disocclusion effects, to view dependent shading and lighting, as well as to prevent layering artefacts with off-axis viewing of layered holograms [17].

For an arbitrary discretized angularly multiplexed layered view structure, such a hologram's total necessary bandwidth<sup>n11</sup> is about  $2.35 \times 10^{11}$  bps (running at 25 fps), which is three orders less than the previously mentioned grid model, and more manageable than addressing every possible voxel.

Based upon this example, we can see how the image-based multi-view holographic rendering algorithm removes redundancies, includes important occlusion and view dependent imagery, and efficiently encodes the 3D information into the holographic fringes. Together with the Fourier–Fresnel technique [30], rapid calculation speeds are achieved. The procedure of the layer-based method is shown in Fig. 4. More details of the algorithm used in this paper and other applications can be found in our previous works [17,31].

The realization of a rapid hologram algorithm using a standard CG rendering pipeline permits the use of standard 3D models, common animation frameworks, and hardware accelerated rendering to create visually rich holographic content. As a result, the algorithm on a single standard graphic processing unit (GPU) can rapidly generate a hologram in seconds with a large information content, greater than  $4 \times 10^8$  bits<sup>n12</sup> per hologram frame, producing visually rich 3D imagery with all relevant 3D cues. .

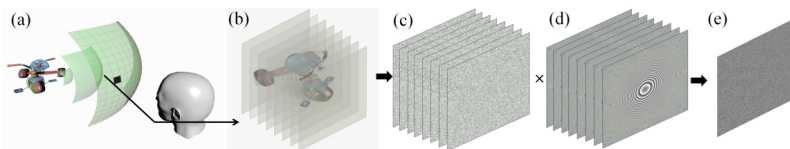


Fig. 4. An illustration of the fundamental concept of angularly tiled layer-based holographic rendering algorithm. (a) The reconstructed holographic image is angularly tiled; (b) Each angular view is sliced along its viewing direction reducing the computation load; (c) Each layer's hologram is calculated from its image slice's Fourier transformation; (d) Corresponding pre-calculated holographic lenses are attached to layers to place each layer at the appropriate depth; (e) The summation of layers becomes the final hologram for this view.

## 7. Apparatus and results

Combining the scanned coarse integral holographic display with the multi-view multi-layer holographic rendering algorithm allows us to display full parallax holographic video. Rendering was performed on a single commodity consumer gaming graphics card (NVIDIA GeForce GTX 460SE). The hologram calculations are conducted using GPUmat, an open-source toolbox allowing MATLAB to run the CUDA library on GPUs.

In Fig. 5(a)-5(f), we show actual holographic images of a 3D model consisting of tricycle displayed on the CIH dynamic display captured from different viewing angles. We also demonstrate the focus cue of a scene consisting of letters, as shown in Fig. 6(a)-6(c). A movie clip showing holographic video of an animated toy tricycle is provided online.

## 8. Discussion

Although the tricycle in Figs. 5(a)-5(g) and characters in Figs. 6 consist of multi-view layered structures, the 3D holographic images appear contiguous. The holographic images maintain a consistent location in space regardless of horizontal or vertical viewpoint. Smooth motion full

parallax is observed with proper occlusion/disocclusion, and without layering or gaps being apparent or appearing with a change in view.

In Fig. 6(a), the camera is focused on the front character X, while the rear character Z is blurred due to camera depth of focus. In Fig. 6(b), the camera is focused on the rear character Z, while the front character X is blurred due to camera depth of focus. Accommodation and vergence are properly coupled.

Currently, the algorithm does not perform in real time, and there are limitations due to data transmission rates in the graphics card. Therefore in our current system, holograms are pre-calculated and uploaded on the device before displaying at a high rate. The SLM control board in use has 4 Gigabytes (GB) on-board memory, and our current system displays 12,600 patterns per second, equal to 1.15 GB per second. Therefore our current system supports 3.4 seconds of holographic video.

In the dynamic CIH display, the scanning system combined with the coarse integral optics allows us to efficiently utilize the SLM's large bandwidth to create a holographic video, especially when compared to other full-parallax holovideo systems (See Table 1). It is expected that a single device, rather than multiple devices, has more immediate potential for increasing a dynamic hologram's effective information content to achieve 10 billion pps. The CIH system also allows the different vertical and horizontal viewing angles to achieve more efficient use of the available information. The reconstructed holographic image is also a real image holding a definitive position in space and accessible for interactive applications.

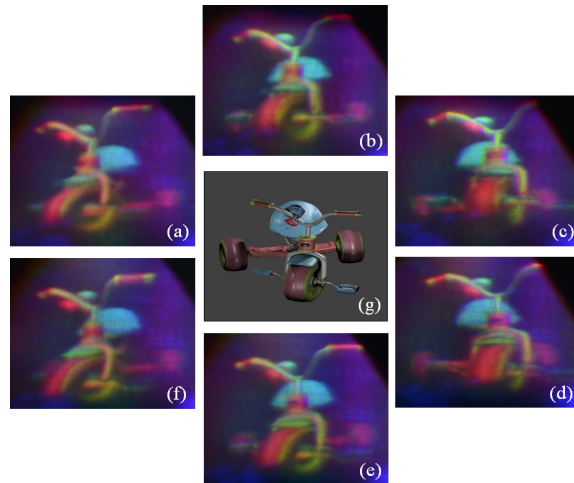


Fig. 5. Captured holographic images (3D tricycle model [32,33]) of the dynamic Coarse Integral Holographic Display system. (a)-(f) Holographic images taken from different viewing angles. (g) Original source computer generated (CG) model rendering. Video results are also provided online.

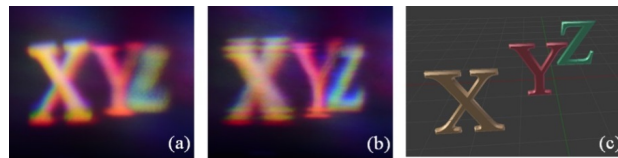


Fig. 6. Focus/accommodation cue tests of the dynamic CIH system. (a)-(b) Images were taken with the camera focused at different depths to show the accommodation cue; (c) The original 3D image source.

As the bandwidth of SLM and scanner technologies improve, holographic displays with a larger wider field of view will be possible. Research will also be needed to further examine the binary hologram's ability to produce a larger number of greyscale voxels.

The layer-based holographic rendering algorithm working in conjunction with the dynamic CIH display enables us to calculate the holograms with all appropriate depth cues, including full-parallax, accommodation cue, occlusion and perspective. The algorithm's rapid speed reduces the computation time for a full holographic frame with all the relevant 3D cues, from theoretically hours or even days down to seconds, even when rendered from a single graphic card. While still not real-time, further optimization, the use of multiple graphics cards, the improvement of GPU computation, and increased data transmission speeds will also lead to the real time holographic video.

## 9. Conclusion

A new holographic display structure – dynamic Coarse Integral Holography, is used to create a video frame rate, full colour, full parallax holographic video display. This structure uses opto-mechanical scanning and coarse integral optics for efficiently reorganizing information from a low SBP high-bandwidth SLM to create dynamic holograms with a large SBP at video rates. An overall hologram frame consisting of 141.6 Megapixels for each of three colours is presented at a frame rate of 23.33 fps, equal to a rate of 10 billion bps from a single display device.

A multi-view multi-layer holographic rendering algorithm (Appendix) works in conjunction with the optical system to further optimise the use of the display's available bandwidth by removing visual and object redundancies, while providing important view dependent cues such as occlusion/disocclusion and being conducive to parallel computation on GPUs.

## Appendix

- n1. For solid angle with a rectangular field of view.  

$$\Omega = (\phi_2 - \phi_1) \times (\cos \theta_2 - \cos \theta_1)$$

$$= \Delta \phi \times (\cos \pi/2 - \cos (\pi/2 - (\theta_2 - \theta_1))), \text{ with } \theta_1 = \pi/2 - (\theta_2 - \theta_1), \theta_2 = \pi/2:$$

$$= \Delta \phi \times \sin \pi/2 \times \sin(\theta_2 - \theta_1)$$

$$\approx \Delta \phi \times \Delta \theta, \text{ for small vertical/polar fields of view:}$$
 where  $\Delta \phi$  is the horizontal/azimuthal diffraction range bound by  $[\phi_1, \phi_2]$  and  $\Delta \theta$  is the vertical/polar diffraction range bound by  $[\theta_1, \theta_2]$  for the rectangular solid angle  $\Omega$  in spherical coordinates.
- n2.  $1,024 \times 768 = 0.78 \times 10^6$   
 n3.  $10.24 \text{ mm} \times 7.68 \text{ mm} \times 1.81^\circ \times 1.81^\circ = 257.64 \text{ mm}^2 \text{deg}^2$   
 n4.  $1,920 \times 1,080 \times 1 \text{ bit} \times 23,148 \text{ Hz} = 47.99 \text{ Gbits/sec}$   
 n5.  $1,920 \times 1,080 \times 8 \text{ bit} \times 100 = 1.66 \text{ Gbits/sec}$   
 n6.  $\sin^{-1}(4 \cdot 0.633/13.68 + \sin(-12^\circ)) - \sin^{-1}(3 \cdot 0.633/13.68 + \sin(-12^\circ)) = 2.654^\circ$  which is close to the same diffraction range when on-axis illumination is used  $\sin^{-1}(1 \cdot 0.633/13.68) = 2.652^\circ$  with only a  $(2.654 - 2.652)/2.654 = 0.07\%$  difference.  
 n7.  $(30 \times 6) \times (1,024 \times 768) = 141.6 \text{ Mega pixels}$   
 n8.  $23.33 \text{ fps} \times 30 \text{ views} \times 6 \text{ views} \times 3 \text{ colours} = 12,600 \text{ frames per second}$   
 n9.  $[23,430 \times 23.33] / [43.4 \times 22,727] = 55.4\%$   
 n10.  $1,024 \times 768 \times 1,000 \times 50 \text{ (horizontal views)} \times 30 \text{ (vertical views)} \times 3 \text{ (colours)} \times 25 \text{ (video rate)} \times 8 \text{ (256 grey levels)} \sim 2.35 \times 10^{14} \text{ bits per second (bps)}$   
 n11.  $(1,024 \times 768) \text{ pixels} \times 50 \text{ horizontal view} \times 30 \text{ vertical views} \times 3 \text{ colours channels} \times 25 \text{ fps} \times 8 \text{ bits per pixel} = 2.35 \times 10^{11} \text{ bps}$   
 n12.  $1,024 \times 768 \times 30 \text{ horizontal views} \times 6 \text{ vertical views} \times 3 \text{ colours} = 4 \times 10^8$

## Acknowledgment

This research was performed through a joint collaboration project between Disney Research and the University of Cambridge through the CAPE consortium. J.S.C. and D.P.C. would like to thank the UK Engineering and Physical Sciences Research Council (EPSRC) for the support through the Platform Grant in Liquid Crystal Photonics (EP/F00897X/1).